ELM mitigation by supersonic molecular beam injection: KSTAR and HL-2A experiments and theory

W.W. Xiao[1,2,3], P.H. Diamond[1,4], W.C. Kim[3], L.H. Yao[2], S.W. Yoon[3], X.T. Ding[2], S.H. Hahn[3], J. Kim[3], M. Xu[4], C.Y. Chen[2], B.B. Feng[2], J. Cheng[2], W.L. Zhong[2], Z.B. Shi[2], M. Jiang[2], X.Y. Han[2], Y.U. Nam[3], W.H. Ko[3], S.G. Lee[3], J.G. Bak[3], J.W. Ahn[5], H.K. Kim[3], H.T. Kim[3], K.P. Kim[3], X.L. Zou[6], S.D. Song[2], J.I. Song[3], Y.W. Yu[7], T. Rhee[1,3], J.M. Kwon[1], X.L. Huang[2], D.L. Yu[2], K.D. Lee[3], S.I. Park[3], M. Jung[3], S. Zoletnik[8], M. Lampert[8], G.R. Tynan[4], Y.S. Bae[3], J.G. Kwak[3], L.W. Yan[2], X.R. Duan[2] and Y.K. Oh[3], J.Q. Dong[2,9], the KSTAR Team and the HL-2A Team

1 WCI Center for Fusion Theory, National Fusion Research Institute, Daejeon, Korea

2 Southwestern Institute of Physics, PO Box 432, Chengdu, People's Republic of China

3 National Fusion Research Institute, Daejeon, Korea

4 University of California, San Diego, 9500 Gilman Drive, La Jolla, CA 92093, USA

5 Oak Ridge National Laboratory, Oak Ridge, TN 37831, USA

6 CEA, IRFM, F-13108 Saint-Paul-lez-Durance, France

7 Institute of Plasma Physics of Academia Sciences, Hefei, People's Republic of China

8 Wigner Research Centre for Physics, Association Euratom, Budapest, Hungary

9 Institute of Fusion Theory and Simulation, Zhejiang University, Hangzhou, People's Republic of China

E-mail: xiaoww@swip.ac.cn; wwxiao@zju.edu.cn

Abstract

We report recent experimental results from HL-2A and KSTAR on ELM mitigation by supersonic molecular beam injection (SMBI). Cold particle deposition within the pedestal by SMBI is verified in both machines. The signatures of ELM mitigation by SMBI are an ELM frequency increase and ELM amplitude decrease. These persist for an SMBI influence time τ_I. Here, τ_I is the time for the SMBI influenced pedestal profile to refill. An increase in $f_{\mathrm{SMBI}}^{\mathrm{ELM}}/f_{0}^{\mathrm{ELM}}$ and a decrease in the energy loss per ELM ΔW_{ELM} were achieved in both machines. Physical insight was gleaned from studies of density and v_ϕ (toroidal rotation velocity) evolution, particle flux and turbulence spectra, divertor heat load. The characteristic gradients of the pedestal density soften and a change in v_ϕ was observed during a τ_I time. The spectra of the edge particle flux $\Gamma\sim <\tilde{v}_r\tilde{n}_e>$ and density fluctuation with and without SMBI were measured in HL-2A and in KSTAR, respectively. A clear phenomenon observed is the decrease in divertor heat load during the τ_I time in HL-2A. Similar results are the profiles of saturation current density J_{sat} with and without SMBI in KSTAR. We note that τ_I/τ_p (particle confinement time) is close to ~1, although there is a large difference in individual τ_I between the two machines. This suggests that τ_I is strongly related to particle-transport events. Experiments and analysis of a simple phenomenological model support the important conclusion that ELM mitigation by SMBI results from an increase in higher frequency fluctuations and transport events in the pedestal.

Keywords: supersonic molecular beam injection (SMBI), ELM mitigation, transport

1. Introduction

H-mode is characterized by an edge pedestal or edge transport barrier (ETB), manifested in the profiles of the plasma density and temperature. In ELMy H-mode, the plasma edge is a region of crucial importance due to its influence on plasma confinement and performance. ELMy H-mode exhibits fast, quasi-periodic short bursts called edge localized modes (ELMs), which eject particles and energy from the plasma. ELM losses will induce significant negative impact on the thermal generation efficiency. It involves the interaction of the large energy impulses released by each ELM with the plasma facing components (PFCs). Depending on the extent of interaction of the ELMs with divertor and main chamber PFCs, material erosion limits require that this energy must be reduced, so as to prevent accelerated degradation of the divertors and wall surfaces [1]. A central question for ITER [2] is whether external control tools can be developed to reduce the ELM size to acceptable values while maintaining good confinement. An effective control scheme should result in an increase in the actual ELM frequency relative to the intrinsic ELM frequency $f_{0\,\mathrm{ELM}}$. Since the relation $f_{\mathrm{ELM}} \times \Delta W_{\mathrm{ELM}} \approx$ const. at constant heating power, with ΔW_{ELM} energy loss per ELM [3], holds for intrinsic ELMs on many diverted tokamaks, increasing the frequency should decrease ΔW_{ELM}, as we desire. Some techniques and physical results are reported in [4], such as the resonant magnetic perturbation (RMP) in DIII-D [5], pellets in ASDEX [6] and DIII-D [7]. Note that, viewed as a physics problem, ELM control is equivalent to tuning the macroscopic oscillations of a self-organized criticality (SOC), which can manifest spatiotemporal chaos and cyclic bursts. In particular, the aim of ELM control is to eliminate the largest transport events, which cause the largest impulsive heat loads on the divertor. In this work, we describe an experimental demonstration of ELM mitigation by supersonic molecular beam injection (SMBI) in HL-2A and KSTAR, and elucidate the physics of this result. The organization of this paper is as follows: the SMBI systems of both machines are introduced in section 2. Section 3 discusses the particle source deposition and the optimized parameters of SMBI pulses. Section 4 presents the basic experimental results. Section 5 describes a simple phenomenological model, which captures some aspects of these results. The importance of τ_I/τ_p is discussed in section 6. Section 7 presents the conclusions and discussions.

2. History of SMBI and its application in HL-2A and KSTAR

An SMBI system was utilized in HL-1 tokamak for the first time [8]. Then it was used for a plasma fuelling study in HL-1M with a formal report in 1998 [9]. Using this method, some interesting physics topics were investigated in different machines, such as fuelling efficiency in ohmic plasma in Tore Supra [10] and in H-mode plasma in NSTX [11], spontaneous particle-transport barrier formation in HL-2A [12] and filament structure change in Heliotron J [13]. SMBI was also used for the ELM mitigation in EAST [14]. On the HL-2A tokamak, the H-mode experiments with SMBI (R = 1.65 m, a-0.5 m, I_P = 140 kA–200 kA, B_T = 1.2–1.5 T, $\langle n_e \rangle \sim (1.8–2.3) \times 10^{19}$ m^{-3}, ECRH heating power ~0.9–1.6MW, NBI heating power~0.3–0.8MW) were performed in 2009 [15]. There are two SMBI systems, on low field side (LFS) and high field side (HFS) [16], respectively, in HL-2A. The SMBI system on LFS was used for ELM mitigation for the first time in 2010. For the SMBI system in LFS, the basic pressure could be 60 bar, and the duration for one SMBI pulse could be more than 0.5 ms. Also, a turbo-molecular pump with the capacity of 450 l s^{-1} was applied to maintain a low background neutral gas pressure during injection [17]. 4ms SMBI pulse duration was used for ELM mitigation experiment in HL-2A [18]. In the KSTAR tokamak, H-mode discharges with NBI and ECRH for diverted plasmas (R—1.8 m, a—0.5 m, κ = 1.8–2.0, B_T = 1.6– 2.4 T, I_p = 0.6–0.7 MA, $\langle n_e \rangle$ = (1.2–4.3)$\times 10^{19}$ m^{-3}) are achieved successfully [19]. The successful experiments of SMBI fuelling and ELM mitigation have been performed in 2011 [20]. The SMBI system was newly installed at a median port of the vacuum vessel to explore ELM mitigation. The SMBI pulses could be performed at room temperature and at

low temperature, ~105 K. The gas pressure range of the SMBI system in KSTAR is from 0.4 to 2.2MPa. 8 and 10 ms SMBI pulse durations were used for ELM mitigation experiments in KSTAR. Figure 1 shows the particle number calibration curve of one SMBI pulse with temperature 105K and gas pressure 1.0MPa. Using this calibration data, the particle number of one SMBI pulse could be estimated in our experiments to be about 5.58×10^{20} and 7.06×10^{20}, respectively. Using these SMBI parameters for KSTAR, the particle location of one SMBI pulse could be at the pedestal foot, in order to achieve ELM mitigation, as shown in figure 6. A similar work on particle number calibration has been reported in HL-2A with different gas temperature and gas pressure [17].

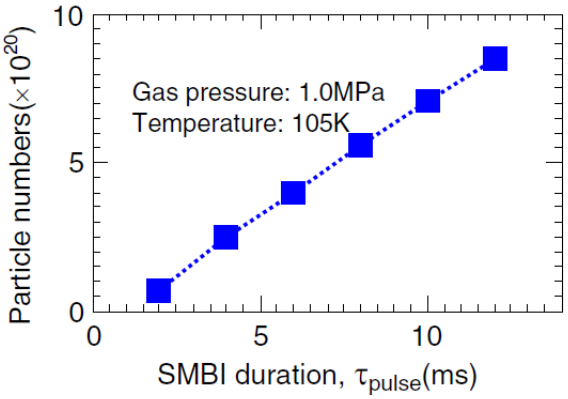

Figure 1. The particle number calibration of SMBI pulse in KSTAR with temperature 105K and gas pressure 1MPa. The definition of the SMBI duration (τ_{pulse}) is detailed in figure 4.

3. Characteristics of the SMBI system for ELM mitigation

3.1. Penetration and particle source position in the pedestal region

As a fuelling tool, SMBI has superior characteristics, such as good local particle deposition [21], good fuelling direction, high gas speed and high fuelling efficiency [22]. A key feature is that the recycling of SMBI is lower than normal gas puffing [16, 22]. These characteristics support trying the experiment of ELM mitigation by SMBI. Local deposition of particles close to the pedestal foot is a central point in this experiment. The local particle source can be determined by the maximum in the time derivative of the density at the beginning of density modulation [21]. Then density evolution is dominated by the particle source. The cold particle source position for one SMBI pulse can be confirmed using the rate of density increase with time, $\partial_t n_e$. In the sameway, deposition of main neutral gas into the pedestal is achieved in H-mode discharges. The particle source position is confirmed, as shown in figure 2, which shows the experimental results for the particle source position and pedestal structure. Figure 2(*a*) shows $\partial_t n_e$ and the square curve is a signal of the SMBI electron magnet valve. The arrow shows the local particle source position at R~ 2.01–2.02 m. The pedestal structure was measured by microwave reflectometry [23]. The density pedestal is about 1.26×10^{19} m^{-3} and the pedestal width is about 3.3 cm. The separatrix position is ~2.03 m, as shown by the dashed line in figure 2(*b*). The third arrow indicates the main particle source position and corresponds to the white arrowin figure 2(*a*). It indicates that the injected cold particles are indeed deposited just inside of the separatrix, as shown in the white ellipse in figure 2(*a*) and the red arrow in figure 2(*b*). It is very clear that the particle source position is shallow and just inside of the separatrix.

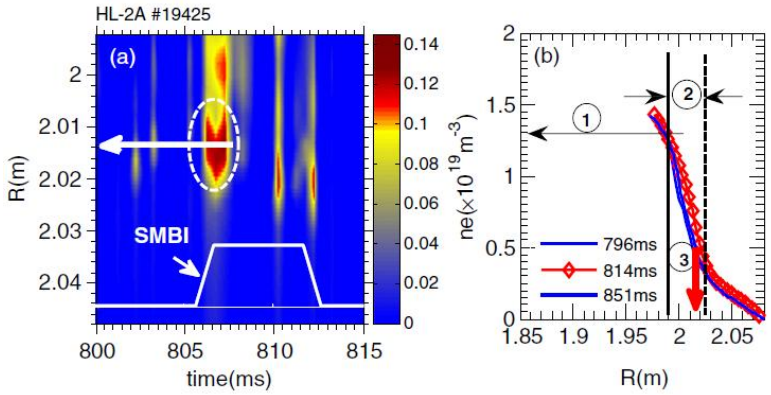

Figure 2. (*a*) is the local particle source position. (*b*) is the pedestal density profiles with and without SMBI. ① is the pedestal top, ② is the pedestal width and ③ is the main particle source position, as shown by the red arrow.

3.2. Optimized parameter of SMBI pulses in HL-2A and in KSTAR

In order to find a set of suitable parameters for SMBI pulses for ELM mitigation experiments, comparative experiments were performed in HL-2A. Optimized SMBI duration in the ELM mitigation experiments has been successfully conducted as shown by figure 3, which presents the relation between individual SMBI pulse duration τ_{pulse} and τ_I, the SMBI persistence influence time. Here, the SMBI influence time τ_I is defined in figure 4, as the time interval from the D_α amplitude decrease or disappearance to the first D_α amplitude recovery. τ_I corresponds to the time needed for the SMBI influenced pedestal profile to refill. For the gas pressure of 1.1MPa in figure 3(*a*), there is no effect of ELM mitigation for 2ms SMBI duration, as shown by the star, while ELM mitigation results appear for 4 and 6ms SMBI duration. However, for gas pressure of 2.0MPa shown in figure 3(*b*), the ELM mitigation effect with 4ms SMBI duration is more striking than that for 2ms SMBI duration. For ELM mitigation by SMBI, the optimized parameters of the SMBI are the gas pressure of 2MPa and the pulse duration τ_{pulse} of 4ms for the HL-2A tokamak. In KSTAR, the gas pressure of the SMBI system is 1.0MPa and the SMBI pulse duration is 8ms for the ELM mitigation experiment. These parameters show that a well defined position of the main particle source (neutral gas) is a prerequisite necessary for the study of ELM mitigation by SMBI. In general, there is no effect of ELM mitigation if the SMBI pulse duration is too short, while there is a strong density increase due to the strong fuelling if the SMBI pulse duration is too long. Thus, a set of suitable parameters for the SMBI pulses in ELM mitigation experiments is very important. The optimized parameters of SMBI pulses in HL-2A and in KSTAR are different. We obtained much longer duration of the persistence influence time in KSTAR than in HL-2A.

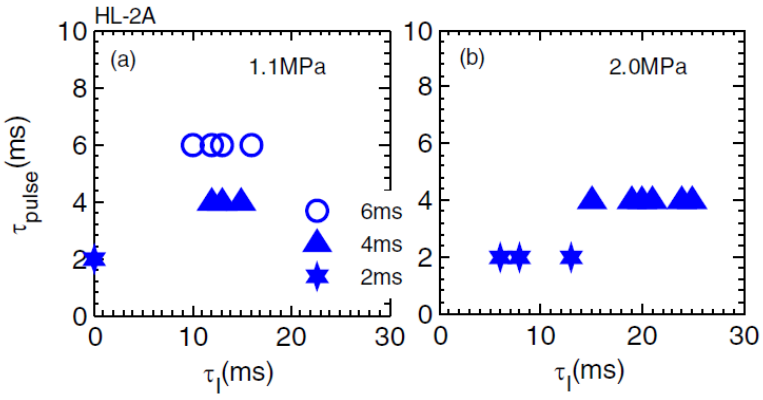

Figure 3. The relation between SMBI duration τ_{pulse} and τ_I in HL-2A.

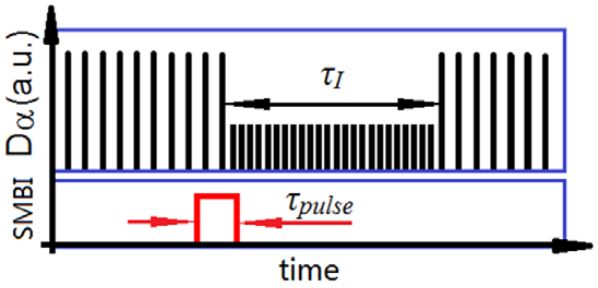

Figure 4. A cartoon showing the definition of the SMBI influence time τ_I in ELM mitigation experiments and the SMBI pulse duration τ_{pulse}.

4. Experiments of ELM mitigation by SMBI in HL-2A and in KSTAR

4.1. Density evolution with and without SMBI

The first experiment on ELM mitigation by SMBI was performed on HL-2A [15]. We observed an ELM frequency increase and an ELM amplitude decrease during an SMBI influence time τ_I for the type III ELMs. The τ_I duration is the time for the SMBI influenced pedestal profile to refill, as shown in the figure above. The τ_{pulse} is the control signal of the SMBI system, corresponding to the SMBI pulse duration. In comparison with the experiment, theτ_I is shown by the double arrows in figures 5(*a*) and (*b*).

In figure 5, the increases in frequency of $f_{SMBI}^{ELM}/f_0^{ELM} \sim 2–3.5$ were achieved in HL-2A and in KSTAR. In particular, the pedestal density gradient scale length is changed during τ_I. The mitigation of large ELMs by SMBI in KSTAR and the type III ELMs in HL-2A are shown in figure 5. Here, (*a*) is the D_α ELM monitor signal of ELM in KSTAR, (*b*) is the D_α ELM monitor and (c) is the density profiles at different times 701, 722, 731 and 737 ms in HL-2A. Density profile analysis indicates a distinct difference in pedestal density gradient steepness is evident upon comparison of profiles with and without SMBI. The density gradient softens immediately following SMBI, while the density gradient without SMBI is steeper than that with SMBI. These correspond to the times indicated in (b) by the arrows. After a τ_I, the steep density gradient state is recovered.

Similar results for the density profile evolution with and without SMBI were observed in KSTAR during ELM mitigation experiments, as shown in figure 6. This shows the density profiles (measured by BES system in KSTAR [24]) at different times for shot 6352. SMBI was injected at 2.7 s. The time of the closed circles is before SMBI injection, and the blue ones are after SMBI. The density gradient slightly softens. The dashed line denotes the separatrix position.

These observations suggest that the pedestal particle confinement is degraded by SMBI. Dramatic results in ELM mitigation by SMBI were achieved in KSTAR [25]. Not only an increase in frequency of $f_{SMBI\,ELM}/f_{0\,ELM} \sim 3.5$ was observed but also the ELM amplitude decreased for a τ_I time of several hundred ms in figure 5(*a*). An experimental indication of ELM mitigation by SMBI is shown by the fact that the ELM frequency increased from 28 to 68 Hz and the ELM amplitude dropped by half, after an SMBI for the large ELMs in KSTAR. The SMBI influence time τ_I is about 400 ms and about 8% of the stored energy is lost with slight confinement degradation.

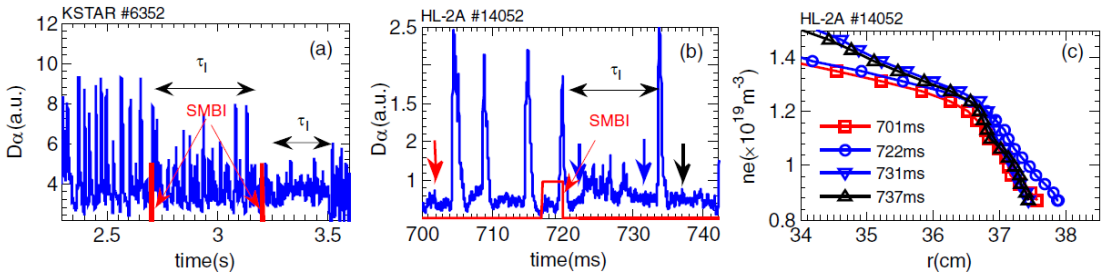

Figure 5. (*a*) is the D_α during ELM mitigation by SMBI in KSTAR. (*b*) is the D_α ELM monitor and (*c*) is the density profiles at different times in HL-2A.

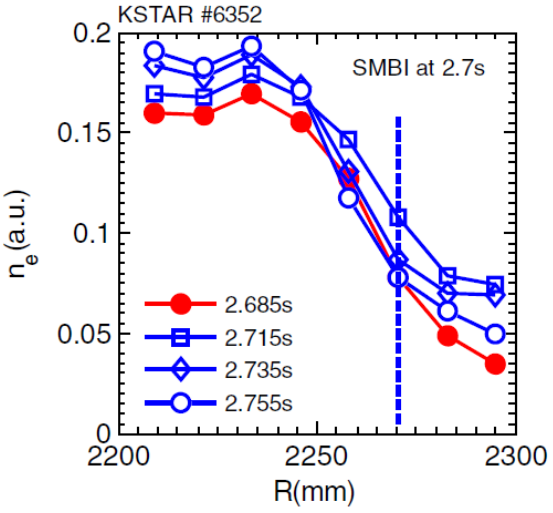

Figure 6. Density profiles by BES measurements. The dashed line means the separatrix by EFIT.

4.2. Toroidal rotation change (v_) with and without SMBI in HL-2A and in KSTAR

A novel critical value of the core rotation velocity $v_{\phi cri} \sim 145$ km s^{-1} was observed at the end of a τ_I period ($\tau_I \sim 320$ ms for shot 6376, $\tau_I \sim 380$ ms for shot 6353) inKSTAR. The ELM amplitude decrease and ELM frequency increase during a τ_I period are shown in figures 7(*a*) and (*c*). The key point is that after each pulse injection, the plasma core toroidal rotation ($v_\_$) decreases sharply, and then slowly recovers or exceeds to a $v_{\_cri}$ at the end of a τ_I period, as shown in figures 7(*b*) and (*d*) by the open blue squares. Before the SMBI, the $v_\phi > v_{\phi cri}$ is observed, as shown by the black dashed lines. After the SMBI, $v_\phi < v_{\phi cri}$ during τ_I, then the core toroidal rotation increases and reaches or exceeds the $v_{\phi\ cri}$ at the end of the τ_I period. It was shown that the density scale gradient length in the pedestal region can be softened by an SMBI pulse injection, as shown in figure 5 by the blue circles and in figure 6 by the blue squares. Another notable effect is that the stored energy decayed slightly, but then it remains constant, as shown by the red curves in figure 7(*b*) and in figure 7(*d*).

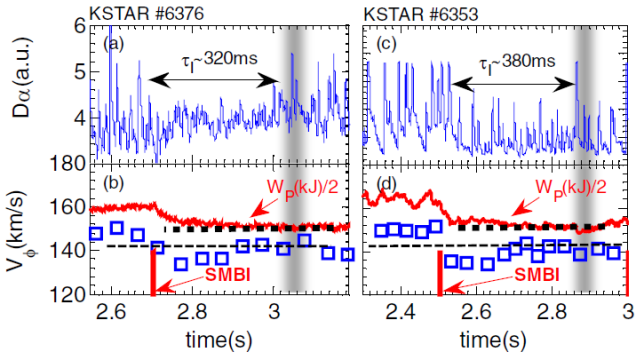

Figure 7. (*a*) and (*c*) are the D_α ELM monitor. (*b*) and (*d*) show the evolutions of v_r and of the stored energy. The grey bars mean the end of τ_I.

The effect on the store energy is then different than on the core toroidal rotation, which drops and then recovers. The phenomenon of the toroidal rotation v_ϕ change with and without SMBIwas also observed for shot 19425 in HL-2A, as shown in figure 8. Figure 8(*a*) shows the evolution of the core and the edge toroidal rotation velocity, which were modulated by multi-SMBI pulses. Figure 8(*b*) is the toroidal rotation profile along the radius. Note that the edge v_r gradient softens (becomes less steep) during a τ_I period, as shown in figure 8(*b*). The edge v_ϕ gradient change in figure 8(*b*) is observed during an SMBI influence time. A similar phenomenon of a density gradient decrease for density in the pedestal region was observed as well, such as in figures 5(*c*) and 6. An approach to a possible explanation was presented in [18, 26, 27]. The key point of this result is that SMBI deposition in the pedestal inhibits the formation of the largest, most extended transport events and ELMs, which span the full width of the pedestal. This scenario implies that during ELM mitigation by SMBI, core toroidal rotation changes because the SMBI softens the edge pressure gradient. Consequently, the magnitude of the ETB electric field shear drops, the ETB momentum confinement, as well as intrinsic rotation drive, also drops [28]. This idea is consistent with the suggestion that the density gradient scale length in the pedestal region softens in response to an SMBI pulse injection as observed in HL-2A and in KSTAR.

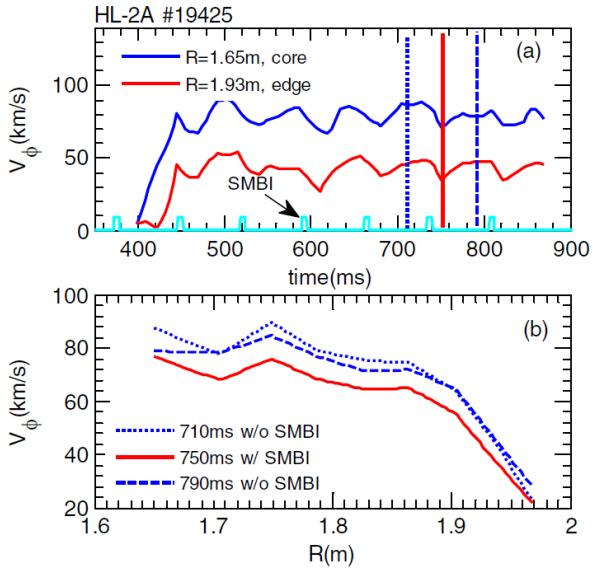

Figure 8. Core and edge toroidal rotation change with and without SMBI for shot 19425 in HL-2A. (*a*) shows the core and edge toroidal rotation velocity modulated by multi-SMBI pulses. (*b*) is the toroidal rotation profiles along radius. The corresponding timing of each profile is noted in (*a*) using the dotted, dashed and full vertical lines.

4.3. Particle flux and density fluctuation analysis at mid-plane in LFS

The particle flux was measured by Langmuir probe (LP) [29] with (the red open squares) and without SMBI (the blue open circles) at the plasma edge and close to the pedestal foot in HL-2A. A change in the spectrum of the edge particle flux $\Gamma\sim <\tilde{v}_r\tilde{n}_e>$ during ELM mitigation by SMBI was observed for shot 16248, as shown in figure 9. Here, $\tilde{v}_r$ is the radial velocity perturbation and $\tilde{n}_e$ is the density perturbation. We see that with SMBI, the low-frequency (f < 10 kHz, grey bar left) content of the edge particle flux spectrum decreases, while there is a slight indication that the higher frequency (f > 10 kHz, grey bar right) content may increase. The change in the edge particle flux suggests that ELM mitigation that could result from an increase in higher frequency fluctuations and transport events in the pedestal [18]. This is not inconsistent with the hypothesis that SMBI inhibits the formation of large (low frequency) avalanches or transport events, while triggering more small (high frequency) avalanches [26, 27]. However, much further work is required to substantiate the hypothesis above. In KSTAR, the spectrum of edge density fluctuations are measured by beam emission spectroscopy (BES) [24, 30] (main vacuum, mid-plane, LFS) in ELM mitigation experiments. Figure 10(*a*) shows the history of the D_α ELM monitor for shot 6352. SMBI was injected at 2.7 s. Figures 10(*b*) and (*c*) show the spectrum of edge density fluctuations. After SMBI, the ELM frequency increases from 28 to 68 Hz and the ELM amplitude drops by more than half. In this shot, the τ_1 is about 400 ms. In figures 10(*b*) and (*c*), the blue curve shows the result without SMBI and the red curve is the analysis with SMBI. The corresponding time windows of the data are marked with the blue and the red bars in figure 10(*a*), respectively. We compare the measurements of the edge density fluctuations obtained from two different BES channels at two different positions.

Fluctuation intensity is measured by BES channel 3 at R =2.248m in figure 10(*b*), close to the pedestal top, from the outside direction. In figure 10(*c*), fluctuation intensity is measured by BES channel 6 at R = 2.277 m, almost at the foot of the pedestal (R_{LCFS} = 2.278 m, by EFIT). There is no distinct difference shown in the density fluctuations in figure 10(*b*), as compared with figure 10(*c*). That means the particle source from SMBI has shallow penetration, SMBI does not reach the top of the pedestal, but only just penetrates to the foot of the pedestal and induces a local density fluctuation increase. The obvious difference is that the low-frequency content of the edge density fluctuation spectrum drops, while the higher frequency content increases. This is shown by the red curve in figure 10(*c*). This is again consistent with the hypothesis that SMBI inhibits the formation of large valanches or transport events, while triggering more small avalanches [18, 26, 27], leading to the increase in $f_{\text{SMBI ELM}}/f_{\text{0 ELM}}$. However, once again, considerable further analysis is required, as the correlation is weak.

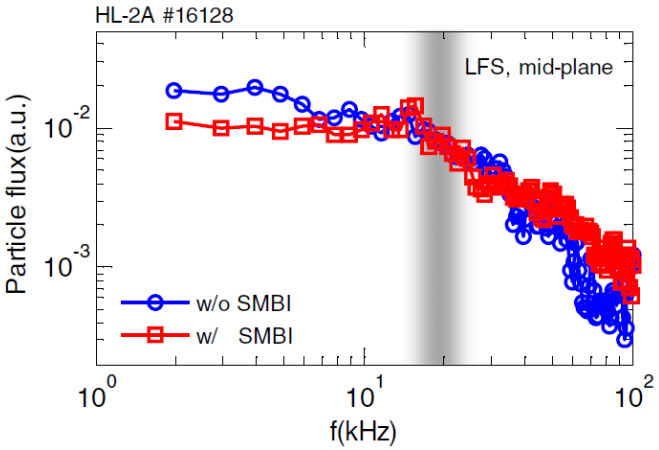

Figure 9. Particle flux measurements for ELM mitigation by SMBI in HL-2A. The particle flux was measured by LP at LFS mid-plane.

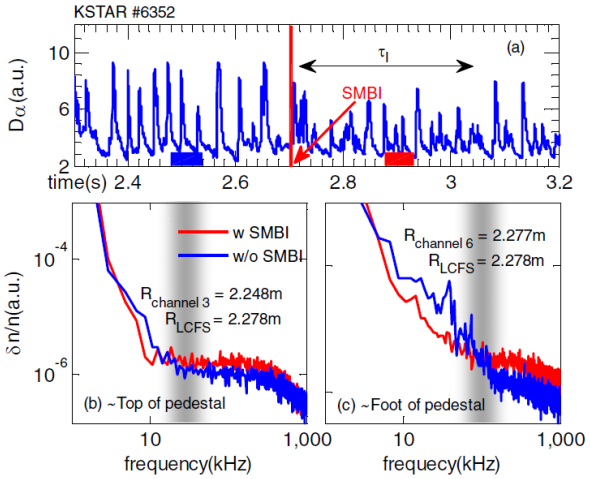

Figure 10. Comparison of the density fluctuation obtained from BES for shot 6352 at two different positions in the pedestal region. The red and blue curves in (*b*) and (*c*) show results with and without SMBI, respectively.

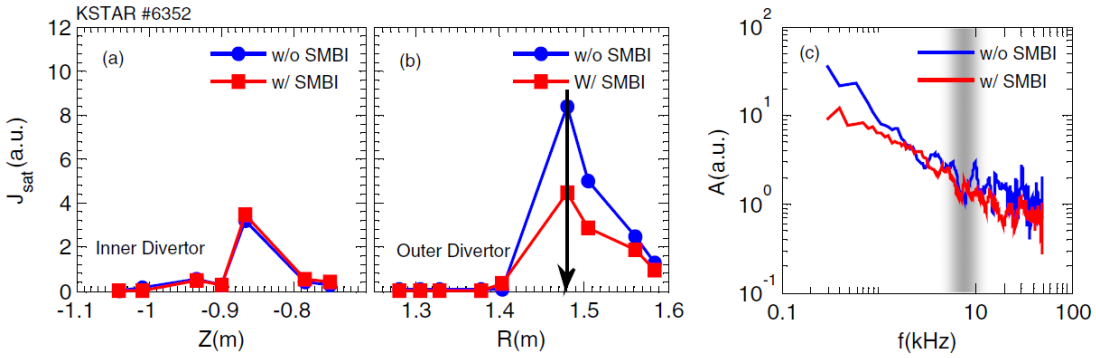

Figure 11. (*a*) is the measurement results by LP in outer divertor with and without SMBI for shot 6352. (*b*) is the spectrum analysis of J_{sat} in KSTAR.

4.4. Divertor signatures of ELM mitigation by SMBI in HL-2A and in KSTAR

The divertor plate is the part of the in-vessel components exposed to the highest heat load. A critical issue for PFCs in tokamaks is the high transient heat loads associated with the type I ELMs, which can lead to rapid erosion of the divertor plates if not addressed. So, a main goal ofELMmitigation is to strongly reduce the ELM energy losses while maintaining adequate confinement. Basic divertor signatures of ELM mitigation by SMBI were observed on the saturation current density profiles J_{sat} and the evolution of the heat loading in divertor. The effect of ELM mitigation by SMBI was investigated using the profiles of the ion saturation current density J_{sat}, which was measured by LP [31] at the inner and outer divertor plates. The profiles of J_{sat} are shown in figures 11(*a*) and (*b*). It is clear that there is almost no change in J_{sat} at the inner divertor with and without SMBI in figure 11(*a*). But, a clear J_{sat} decrease was observed at the outer divertor with SMBI, as shown in figure 11(*b*) by the closed red squares. Here, $J_{sat} \sim Cn_eT_{0.5\,e}$ for $T_e >> T_i$ (C is a constant, n_e is density and T_e is electron temperature). Since $n_e = \langle n_e \rangle + \tilde{n}_e$, this means there is a relation between J_{sat} and particle flux $\Gamma \sim \langle \tilde{v}_r \tilde{n}_e \rangle$. The particle flux drops strongly (almost halved) with SMBI, in comparison with the case without SMBI. This outcome is consistent with the aim of the ELM mitigation, i.e. to decrease the energy load on the divertor or distribute the load on the divertor over a larger area. Figure 11(*c*) shows the spectrum analysis J_{sat}, as observed during ELM mitigation experiments. The chosen data of the LP are marked using the line arrow in figure 11(*b*). A comparison of amplitude of the J_{sat} is shown in figure 11(*c*), for both cases as the red curve and the blue curve. Results suggest that with SMBI, the

spectrum of the low-frequency content (f < 10 kHz, grey bar left) clearly decreases. Information on the high-frequency content of J_{sat} is limited by the probe sampling frequency. The results of the spectrum analysis of J_{sat} suggest the conclusion that the main contribution of drop of the particle flux in figure 11(*b*) is from the decrease in the low-frequency region in figures 9 and 10(*b*). Divertor heat load was successfully reduced in HL-2A, as shown in figure 12. The heat load during ELM mitigation by SMBI was measured by LP [29]. This result shows the heat load evolution with time, with and without SMBI. Figure 12(*a*) is the D_α ELM monitor signal and (b) is the heat load evolution with time. An SMBI pulse was injected at 500 ms. The ELM frequency increases and amplitude decreases during a τ_l (~25 ms), as shown in figure 12(*a*). During the τ_l time, the heat load on the divertor was reduced and recovered slowly at the end of τ_l (the colour bar means the heat power intensity). A reduction in the ELM peak heat flux as the ELM size decreases is observed. It is consistent with the change in the J_{sat} with and without SMBI in figure 11(*b*) in KSTAR. Thus, this means the divertor target material could be prevented from eroding by the larger ELMs. hese results illustrate directly that it is possible to mitigate divertor heat load through the ELM mitigation by SMBI.

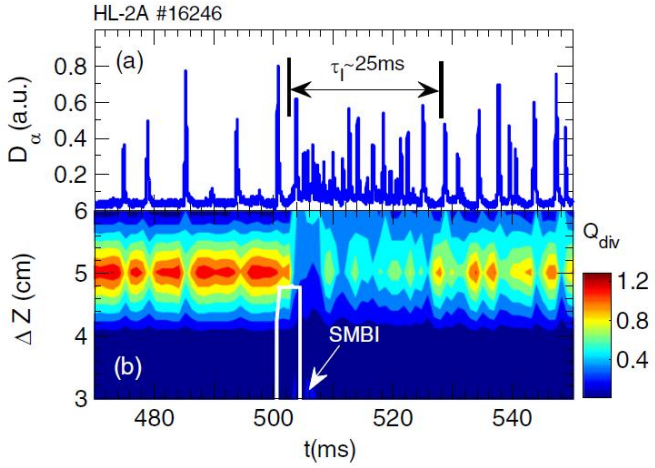

Figure 12. Heat load evolution with and without SMBI for shot 16246 in HL-2A. The colour scale represents the Q_{div} in MWm^{-2}.

5. Phenomenological model of results

A simplified model study using a bi-stable cellular automata model was used to elucidate the physics of the hallow particle deposition effect of SMBI on ELM mitigation [27]. Through the sand-pile model study, it was shown that shallow particle deposition induced frequent small ejection which prevented the occurrence of large crashes. For deep particle deposition, the mitigation of large crashes was rarely observed. The basic model is described in [26] and consists of a sand pile with an ejecting boundary on one side, a bi-stable toppling rule, noise-driven scattering to emulate collision diffusion, and an ultimate upper hard threshold on the occupation density for relaxation of the gradient, to emulate MHD the trigger for ELM events. Here, the bi-stable toppling rule for the pile captures several basic aspects of L and H phase turbulent transport. The hard threshold models an upper limit on profile steepness, as in a $(\nabla p)_{crit}$ for MHD instabilities [32], frequently associated with ELMs. The reader is referred to [26] for further details of the model. In the model, actual edge discharge occurs when the entire edge pedestal region is populated up to the hard threshold limit, and appears as an ejection event driven by avalanches, which span the full pedestal cross-section. The trends indicated by this simplified model study are all qualitatively consistent with the experimentally observed trends, and suggests that shallow SMBI deposition into the pedestal can mitigate ELMs by reducing the population of large avalanche transport events, while increasing the number of smaller events. SMBI does

this by stimulating localized fluctuations around the deposition point, which act to 'break up' large avalanches, and convert them to smaller ones. Although this simple extended SOC model is conceptually appealing and has several qualitative successes, we note here that is premature to claim too much from it. In particular, measurements of fluctuations, pedestal ion and electron temperature measurements in KSTAR and in HL-2A were not available. As a result, MHD stability analysis of the pedestal was not possible. Thus, considerable further study and analysis are required to strongly substantiate the phenomenological model based interpretation given here.

6. Importance of τ_I/τ_p in ELM mitigation by SMBI

In ELM mitigation by SMBI, it was observed that the τ_I is about 15–25 ms in HL-2A and about 250–400 ms in KSTAR, respectively. It is indeed quite different in the two machines. τ_I is close to the τ_E in HL-2A (τ_E ~ 20–30 ms) but much larger than the τ_E in KSTAR (τ_E ~ 120–170 ms [33]). Ohmic particle confinement improvement is described by anH_p factor ($H_p = \tau_p/\tau_E$) and the τ_p is defined by theoretical analysis [34]. For the H-mode case, the relationship between the τ_p and the τ_E was examined. The ratio of τ_p to τ_E is about 1 in the low density regime (linear confinement region), but for the high line-averaged density regime, this ratio is larger than 2 [35]. It was shown that τ_p depends strongly on the line-averaged density, while the dependence of τ_E on density is weaker [35]. In order to understand the behaviour of τ_I/τ_p in ELM mitigation by SMBI, we distinguish experiments in the low line-averaged density regime and the high line-averaged density regime, corresponding to HL-2A (n_e ~ (1.5–2) × 10^{19} m^{-3}) and KSTAR (n_e ~ (3.3–3.8) × 10^{19} m^{-3}), as shown in figure 13. In figure 13, the lowline-averaged densitywas shown using the blue ellipse (τ_I/τ_E~ 1), and the high line-averaged density regime is shown using the red ellipse (τ_I/τ_E ~ 2–3). It is helpful to understand the physics of τ_I/τ_p, i.e. the long or short τ_I results from particle confinement, in other words, we want to know whether there exists an approximate constant ratio of τ_I/τ_p. An estimated ratio of τ_p/τ_E is about 1 in 1.8 × 10^{19} m^{-3} in HL-2A, and the ratio of τ_p/τ_E is about 2.4 in 3.5×10^{19} m^{-3} in KSTAR.We can get the ratio of τ_I/τ_p ~ 1 with an averaged τ_I of 20 ms in HL-2A (τ_p/τ_E ~ 1), and also get the ratio of τ_I/τ_p ~1 with an averaged τ_I of 300 ms in KSTAR (τ_p/τ_E ~ 2.4). That means there would be an approximately constant ratio of τ_I/τ_p in both machines, i.e. τ_I/τ_p ~1. It indicates that the contributions of the SMBI persistence or influence time τ_I is dominated by the particle confinement, thus the particle-transport events play important roles in the ELM mitigation by SMBI.

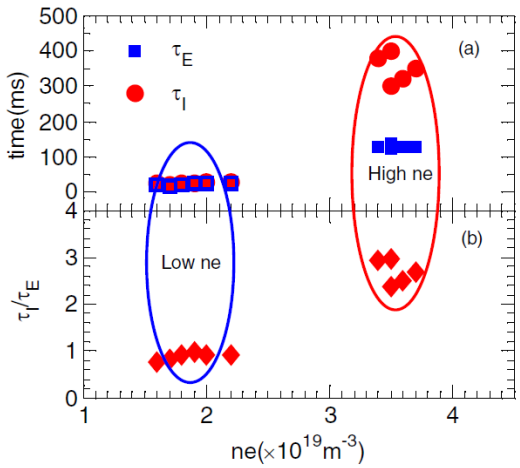

Figure 13. τ_E, τ_I and τ_I/τ_E in HL-2A and in KSTAR. (*a*) is the experimental results of τ_I and τ_E and (*b*) is the ratio of τ_I/τ_E in HL-2A and in KSTAR. The low line-averaged density is shown using the blue ellipse, τ_I/τ_E ~ 1, and the high line-averaged density is shown using the red ellipse, τ_I/τ_E ~ 2–3.

7. Conclusions and discussions

ELM mitigation by SMBI pulse injection into the pedestal region was achieved in two different machines, HL-2A and KSTAR. An increase in $f_{\mathrm{SMBI}}^{\mathrm{ELM}}/f_{0}^{\mathrm{ELM}} \sim 2$–3.5 and a decrease in the energy loss per ELM ΔW_{ELM} were achieved in both machines. These experimental results show that the frequency and the amplitude of ELMs can be actively controlled by SMBI using an SMBI pulse of optimized duration and achieving good local particle deposition (close to the pedestal foot, with shallow penetration depth). Interpretations of physical observations were presented:

(i) The characteristic slopes of the pedestal density were softened during a τ_{I} time and the $v_{\_}$ drops at the time of injection of SMBI and then recovers at the end of τ_{I}.

(ii) The spectra of the edge particle flux was measured by Langmuir probes with and without SMBI in HL-2A. Similar results were obtained for the edge density fluctuation by BES in KSTAR. We see that with SMBI, the low-frequency (f < 10 kHz) content of the edge particle flux spectrum decreases. The change in the edge particle flux suggests that ELM mitigation may result from an increase in higher frequency fluctuations and transport events in the pedestal.

(iii) The analysis of the J_{sat} amplitude in the divertor shows that with SMBI, the low-frequency content of the spectrum (f < 10 kHz) decreases. One conclusion of the change in J_{sat} indicates the main contribution of the drop of the particle flux is from the decrease in the low-frequency region.

(iv) Clearly, the divertor heat load decreased during a τ_{I} time, as measured in HL-2A. This is consistent with the profiles of saturation current density J_{sat} with and without SMBI in KSTAR.

An interesting observation is that the ratio $\tau_{\mathrm{I}}/\tau_{\mathrm{p}}$ is close to 1. It suggests that τ_{I} is strongly related to the behaviour of particle-transport events during ELM mitigation by SMBI. Experiments and the simple extended SOC model support the important conclusion that ELM mitigation by SMBI results from an increase in higher frequency fluctuations and transport events in the pedestal, and the SMBI inhibits the occurrence of large transport events which span the entire pedestal width. However, considerable further work is required to substantiate this hypothesis. It also indicates that there would be an approximately constant ratio $\tau_{\mathrm{I}}/\tau_{\mathrm{p}} \sim 1$ in both machines. This suggests the contributions of τ_{I} are set by the particle transport events, which regulate pedestal building and refilling after SMBI. It should be noted that two important physics topics are highlighted by the experiments of ELM mitigation by SMBI. The physics issues of the ELM mitigation by SMBI will be studied in the future:

(i) The role of the turbulence and zonal flow(ZF) for pedestal particle transport should be investigated in connection with the role of transport in ELM mitigation by SMBI. Density fluctuation amplitude and edge poloidal rotation velocity in the pedestal can be obtained by BES and Doppler backscattering (DBS)/reflectometry systems. This will allow us to understand the relations between the turbulence and particle transport, i.e. which turbulence will dominate and so determine a particle pinch, and which turbulence will drive the adverse sign of the pinch velocity. We will examine whether there is a possible feedback loop here. This question is related to the density perturbation induced by SMBI. For example, SMBI pulse injection can change the local density profiles causing a change in ZF damping. This will result in a turbulence increase and a transport increase. This scenario is some explanation of ELM mitigation by SMBI. It merits investigation. In this paper, we have mentioned that the physics of ELM mitigation by SMBI is related to the local density profiles, the turbulence and the transport during the SMBI duration. It indicates that determining how to explore the relations among the collisionality [36], turbulence and ZF [37] and the profiles (n_{e}, T_{e} and T_{i}) with and without SMBI is a key point to the next step study. Understanding of this topic is helpful to know pedestal particle transport in the ELM mitigation phase.

(ii) To explore the sensitivity of the response time of the central toroidal velocity to edge perturbations is

another interesting topic of the ELM mitigation by SMBI. Probing intrinsic torque in the pedestal region and understanding the response time of the ΔV_φ from the edge to the core due to edge local perturbations, as shown in figures 7 and 8, are very interesting. But, how fast the response of V_φ is remains an open issue. In the H-mode phase, it was noted that a SMBI perturbation in the plasma edge could induce a fast change (decrease) in V_φ in the core plasma. It means that the global toroidal V_φ decreased during the short perturbation time. But the decrease in the toroidal rotation in core plasma $V_{\varphi 0}$ is very sensitive to the edge plasma conditions, and related to them by a fast response from the edge to the core. All of these will be explored in future work of the ELM mitigation by SMBI.

Acknowledgments

This work was supported by the World Class Institute (WCI) Program No WCI 2009-001, the KSTAR project and World Leading Institute (WLI) program, NRF Korea No 2012–4836, China National Fusion Project for ITER under Grant No 2009GB104007, the NSFC Nos 11175056 and 10975049, DOE Grant DE-FG02-04ER54738 and China-Korean joint foundation under the Grant No 2012DFG02230.

References

[1] Loarte A. *et al* 2003 *Plasma Phys. Control. Fusion* **45** 1549

[2] ITER Physics Basis Editors 1999 *Nucl. Fusion* **39** 2137

[3] Herrmann A. 2002 *Plasma Phys. Control. Fusion* **44** 883

[4] Evans T.E. 2013 *J. Nucl. Mater.* **438** S11–8

[5] Evans T.E. *et al* 2008 *Nucl. Fusion* **48** 02400

[6] Lang P.T. *et al* 2012 *Nucl. Fusion* **52** 023017

[7] Baylor L.R. *et al* 2013 *Phys. Rev. Lett.* **110** 245001

[8] Yao L. *et al* 1993 Molecular beam injection in the HL-1 tokamak *20th EPS Conf. on Controlled Fusion and Plasma Physics (Lisboa, Portugal,1993)* vol 17C(I) (Geneva: European Physical Society) p 303

[9] Yao L.H. *et al* 1998 *Nucl. Fusion* **38** 631

[10] P ́egouri ́e B. *et al* 2003 *J. Nucl. Mater* **313–316** 539

[11] Soukhanovskii V.A. *et al* 2007 *J. Nucl. Mater.* **363–365** 432–6

[12] Xiao W.W. *et al* 2010 *Phys. Rev. Lett.* **104** 215001

[13] Mitzuuchi T. *et al* 2012 *Proc. 24th Int. Conf. on Fusion Energy 2012 (San Diego, CA, 2012)* [EX/P3-07] www-naweb.iaea.org/napc/physics/FEC/FEC2012/index.htm

[14] Zou X.L. *et al* 2012 *Proc. 24th Int. Conf. on Fusion Energy 2012 (San Diego, CA, 2012)* [PD/P8-08] www-naweb.iaea.org/napc/physics/FEC/FEC2012/index.htm

[15] Duan X.R. *et al* 2010 *Nucl. Fusion* **50** 095011

[16] Yao L.H. *et al* 2007 *Nucl. Fusion* **47** 1399

[17] Chen C.Y. *et al* 2010 *J. Plasma Fusion Res. Ser.* **9** 37–42

[18] Xiao W.W. *et al* 2012 *Nucl. Fusion* **52** 114027

[19] Kwon M. *et al* 2011 *Nucl. Fusion* **51** 094006

[20] Kim J. *et al* 2012 *Nucl. Fusion* **52** 114011

[21] Xiao W.W. *et al* 2010 *Rev. Sci. Instrum.* **81** 013506

[22] P ́egouri ́e B. *et al* 2007 *Plasma Phys. Control. Fusion* **49** R87

[23] Zhong W.L. *et al* 2011 *Rev. Sci. Instrum.* **82** 103508

[24] Nam Y.U., Zoletnik S., Lampert M. and Kovacsik A. 2012 *Rev. Sci. Instrum.* **83** 10D531

[25] Xiao W.W. *et al* 2012 *Proc. 24th Fusion Energy Conf. (San Diego, CA, 2012)* (Vienna: IAEA) EX/6-3Ra www-naweb.iaea.org/napc/physics/FEC/FEC2012/html/fec12.htm

[26] Gruzinov I., Diamond P.H. and Rosenbluth M.N. 2002 *Phys. Rev. Lett.* **89** 25

[27] Rhee T., Kwon J.M., Diamond P.H. and Xiao W.W. 2012 *Phys. Plasmas* **19** 022505

[28] Diamond P.H. *et al* 2013 *Nucl. Fusion* **53** 104019

[29] Yan L.W. *et al* 2005 *Rev. Sci. Instrum.* **76** 093506

[30] Guszejnov D. *et al* 2012 *Rev. Sci. Instrum.* **83** 113501

[31] Bak J.G. *et al* 2010 *Contrib. Plasma Phys.* **50** 892

[32] Xu X.Q. *et al* 2010 *Phys. Rev. Lett.* **105** 045004

[33] Yoon S.W. *et al* 2011 *Nucl. Fusion* **51** 113009

[34] Staib P. 1982 *J. Nucl. Mater.* **111** 109

[35] Takenaga H. *et al* 1995 *Nucl. Fusion* **35** 853

[36] Lin Z. *et al* 1999 *Phys. Rev. Lett.* **83** 3645

[37] Diamond P.H. *et al* 2005 *Plasma Phys. Control. Fusion* **47** R35